Longitudinal and Lateral Thermal Dispersion in Packed Beds

Part II: Comparison between Theory and Experiment

J. LEVEC

Department of Chemistry and Chemical Technology
University of Ljubljana
Ljubljana, Yugoslavia

and

R. G. CARBONELL

Department of Chemical Engineering
North Carolina State University
Raleigh, NC 27695

The thermal response of a packed bed subject to step changes in fluid temperature was measured in the Peclet number range from 10 to 10^3. Fluid temperature and particle temperatures were measured independently at six different axial locations in the bed as a function of time. From the temperature breakthrough curves we were able to calculate the spatial separation between the fluid and solid temperature fronts. The measured values were higher by a factor of 2 to 3 than those predicted by traditional heat transfer models. Longitudinal effective thermal conductivities were also computed and compared to theoretical predictions. The new heat transfer model developed in a previous paper is able to account for these differences between experimental results and the predictions of the dispersion-concentric and continuous solid phase models used by previous investigators. Steady-state experiments were used to measure lateral effective thermal conductivities. A temperature gradient was imposed at the top of the bed perpendicular to the flow direction and its spread was measured at different axial locations in the Peclet number range from 10 to 10^3. The predicted lateral effective thermal conductivities calculated using mass transfer data to estimate the hydrodynamic dispersion effect were significantly lower than the measured values. This is possibly due to the influence of viscosity and density gradients in the flow field in the packed bed.

SCOPE

In Part I of this work we derived a new model for heat transfer in packed beds using the method of spatial averaging. This new model has convective and dispersive coupling terms which are not present in the more traditional analyses of heat transfer in packed beds, such as the continuous solid phase model and the dispersion-concentric model (Wakao et al. 1979). By studying the transient response of the transport equations for the average temperature of fluid and solid to a pulse disturbance, we were able to draw several conclusions which can be tested experimentally. The first is that given a sufficiently long time, the pulses of temperature in the fluid and solid phases will move at a constant and equal velocity, and as a result will remain separated by a constant distance. This distance is strongly influenced by the magnitude of the convective coupling terms. Using reasonable estimates for the terms in the expression for the separation distance between pulses, it is possible to show that if our model is correct the experimentally measured pulse separations will be larger than those predicted by the continuous solid phase or the dispersion-concentric model. One of the main objectives of this work is to measure the response of a packed bed to step changes in fluid temperature. In doing this, we will be measuring the temperature response of the fluid and the solid independently at various axial locations. This will allow a direct measurement of the separation distance between the response of the fluid and the solid particles. This measured separation distance can then be compared to the predictions of the theory for a wide range of Peclet numbers (10 to 10^3).

The second conclusion drawn from the analysis is that for these long times since the input disturbance, the temperature pulses in the fluid and solid phases will spread about their centroids at constant and equal rates. This helps to define an axial or longitudinal effective thermal conductivity under flow conditions which contains three major contributions: a purely conductive term, a hydrodynamic dispersion term, and a term accounting for pulse spread due to the time lag associated with heat conduction into the particles. Estimates made of these contributions allow a direct comparison with experimental data. From the measured temperature response of the fluid and solid we can compute an experimental longitudinal effective thermal conductivity which is then compared to the theoretical expression in the previous paper, again in the Peclet number range from 10 to 10^3.

The third conclusion which could be drawn from the model equations is that steady state effective thermal conductivities in packed beds are likely to be quite different from effective thermal conductivities measured under transient conditions due

Work performed while the authors were at the Department of Chemical Engineering, University of California, Davis, CA 95616.

to the fact that under steady state conditions the fluid and the solid are in local thermal equilibrium. Lateral effective thermal conductivities are normally measured in steady state experiments, and as a result we derived an expression for the effective thermal conductivity in the direction perpendicular to flow which contained contributions from conduction and hydrodynamic dispersion. Estimates of these contributions were made which again can be tested experimentally. We devised a steady state experiment to allow direct calculations of the lateral effective thermal conductivity by measuring the spread of a temperature gradient imposed perpendicular to the flow direction at various axial locations. This technique does not involve heating the column from the wall, and as a result lateral effective conductivities do not have to be deduced by subtracting the effect of the wall heat transfer resistance. Lateral effective conductivities were measured in the Peclet number range from 10 to 10^3 and were compared with the analytical expression.

CONCLUSIONS AND SIGNIFICANCE

Transient step response experiments were carried out in a packed bed in the Peclet number range from 10 to 10^3. The temperature response of the fluid and the solid phases were measured independently at six different axial locations in the bed. From these data we were able to compute the velocity of the temperature disturbance in the fluid and solid phases. If a previously derived length criterion (Eq. 19) was satisfied, the velocities of the temperature disturbances in the two phases were found to be equal. This velocity compared extremely well with the predicted value given in Eq. 3. The thermal dispersivities calculated from the fluid and solid phase temperature responses were also equal, in agreement with Eq. 11.

By calculating the mean residence time for the temperature disturbance of the fluid phase and the solid phase at a fixed axial location, it was possible to calculate the spatial separation between the fluid and solid phase temperature waves. The experimental values for this quantity were found to be a factor of 2 to 3 larger than those predicted by the traditional heat transfer models and given in Eq. 29. The explanation for this is that the additional convective coupling terms in the new heat transfer model of Levec and Carbonell (1985) contribute significantly to this separation between fluid and solid temperature responses, as shown by Eqs. 5 and 30. This is in agreement with the theoretical predictions made by Zanotti and Carbonell (1984) in their study of transient heat transfer in a capillary tube with conducting walls.

The transient longitudinal effective thermal conductivities could be predicted fairly accurately using the results in Eq. 14. If experimental values of the separation between fluid and solid temperature responses are used in estimating the heat exchange contribution to the thermal spread, the predicted values lie above the data. If we use the results of the continuous solid phase or the dispersion-concentric heat transfer models to estimate the pulse separation, the prediction lies a little below the data. Additional analysis needs to be done in order to determine the exact reason for the difference between theory and experiment, but one possibility is the fact that in Eq. 14 we have neglected terms in the heat exchange contribution to dispersion arising from the closure scheme developed in the previous paper. These terms could reduce the calculated values of the longitudinal effective thermal conductivity sufficiently to improve the agreement between theory and experiment.

Steady state experiments were carried out in order to measure lateral effective thermal conductivities in the Peclet number range from 10 to 10^3. This was done by direct measurement of the spread of a temperature gradient prependicular to the flow direction as a function of axial location in the bed. The measured lateral effective thermal conductivities were significantly larger at Peclet numbers near 10^3 than those predicted by Eq. 17. In Eq. 17 we attempt to estimate the lateral effective thermal conductivity from mass transfer data. However, this does not take into account the coupling between heat conduction in the particles and hydrodynamic dispersion in the fluid phase. It also assumes that the flow fields in the two cases are identical. However, since temperature gradients in the bed lead to significant changes in fluid density and viscosity, it is likely that the flow field in the region of high temperature gradients is quite different from the flow field of a fluid with a high gradient of solute which is found at very low concentration. The ratio of longitudinal to lateral effective thermal conductivities can take on very large values at high Peclet numbers. This is due to the fact that the longitudinal conductivites are measured under transient conditions and the heat contribution to axial spread is strongly dependent on the Peclet number. Lateral effective thermal conductivities measured in steady state experiments only exhibit a hydrodynamic dispersion contribution to the spread, which is much less dependent on Peclet number.

INTRODUCTION

This paper deals with the experimental determination of longitudinal and lateral effective thermal conductivities in packed beds in the Peclet number range from 10 to 10^3. The longitudinal effective thermal conductivity is measured using a transient step response experiment (Gunn and de Souza, 1974; Yagi et al., 1960), while the lateral effective thermal conductivity is measured under steady state conditions. We shall not attempt a complete literature survey of this vast area here, but we refer the reader to two recent articles (Dixon and Cresswell, 1979; Wakao et al., 1979) which have summarized some of the most significant work.

Two experimental aspects distinguish our work from previous contributions. The first is that in our measurements of longitudinal effective thermal conductivities, we measure the response of the fluid phase and of the solid particles independently at various axial locations. In this way we can not only measure the longitudinal effective thermal conductivity, but also measure the separation or lag between the response of the fluid and the solid phases to the step disturbance. This separation has been estimated in the previous paper using the new heat transfer model, and these measurements provide an opportunity to test theory and experiment. The second new aspect of this work involves the method of measurement of the lateral effective thermal conductivities. This is done in a steady state experiment where a temperature gradient perpendicular to the direction of flow is imposed at the top of the bed. Special thermocouple banks are arranged to measure the temperature profile perpendicular to the bed axis at different axial locations. From the lateral spread of the temperature profiles we can compute directly the lateral effective thermal conductivity. This is an improvement over previous techniques which involve heating the walls of the column. In order to determine lateral effective thermal conductivities one then needs to estimate wall heat transfer coefficients which are subject to large sources of experimental error (Gunn and Khalid, 1975; Kunii and Ono, 1968). In the section that follows we summarize the theoretical results that are to be tested experimentally. We then discuss the experimental techniques and the comparison between theory and experimental measurements.

RESULTS OF HEAT TRANSFER MODEL

Longitudinal Effective Thermal Conductivity

Consider a pulse or step disturbance in fluid temperature that is introduced uniformly into the cross section of a packed bed at time $t = 0$. After a sufficiently long time had passed since the introduction of the disturbance, it was shown in the previous paper that the equations for the fluid and solid phase average temperature would reduce to the form

$$\frac{\partial\langle T_\beta\rangle^\beta}{\partial t} + u_\beta\frac{\partial\langle T_\beta\rangle^\beta}{\partial z} = (\alpha^*_{zz})_\beta\frac{\partial^2\langle T_\beta\rangle^\beta}{\partial z^2} \tag{1}$$

and

$$\frac{\partial\langle T_\sigma\rangle^\sigma}{\partial t} + u_\sigma\frac{\partial\langle T_\sigma\rangle^\sigma}{\partial z} = (\alpha^*_{zz})_\sigma\frac{\partial^2\langle T_\sigma\rangle^\sigma}{\partial z^2}. \tag{2}$$

Here u_β and u_σ are the pulse velocities in the fluid and solid phases, and $(\alpha^*_{zz})_\beta$ and $(\alpha^*_{zz})_\sigma$ are longitudinal effective thermal dispersivities for the fluid and solid. When Eqs. 1 and 2 apply, the pulse velocities are equal and given by

$$u = u_\beta = u_\sigma = \frac{\langle v_\beta\rangle^\beta}{1+K} \tag{3}$$

where K is the ratio of heat capacities

$$K = \frac{\epsilon_\sigma(\rho c_p)_\sigma}{\epsilon_\beta(\rho c_p)_\beta} \tag{4}$$

The temperature pulses in the fluid and solid phases are separated by a distance Δ given by

$$\frac{\Delta}{d_p} = \frac{1}{6}\frac{Pe_p}{Nu}\left(\frac{K}{1+K}\right) - \frac{(S_{\beta\beta}+S_{\beta\sigma})}{Nu} \tag{5}$$

where Nu is a Nusselt number based on an overall heat transfer coefficient

$$\frac{1}{Nu} = \frac{1}{Nu_f} + \frac{1}{10\kappa} = \frac{k_\beta}{Ud_p} \tag{6}$$

The second term on the righthand side of Eq. 5 is the contribution from the convective coupling terms. According to a capillary tube model for the heat transfer process, these additional terms are of the order (Zanotti and Carbonell, 1984)

$$-\frac{S_{\beta\beta}}{Nu} = \frac{1}{216}Pe_p\left(\frac{\epsilon_\beta}{\epsilon_\sigma}\right); \qquad S_{\beta\sigma} = 0. \tag{7}$$

The Peclet number and the Nusselt number Nu_f in the above equations are defined as

$$Pe_p = \frac{\langle v_\beta\rangle^\beta d_p}{\alpha_\beta}\left(\frac{\epsilon_\beta}{1-\epsilon_\beta}\right) \tag{8}$$

and

$$Nu_f = \frac{h_f d_p}{k_\beta} \tag{9}$$

respectively. The quantity κ is the ratio of solid to fluid conductivities

$$\kappa = k_\sigma/k_\beta \tag{10}$$

The longitudinal dispersivities for the fluid and solid are equal for long times

$$\alpha^*_{zz} = (\alpha^*_{zz})_\beta = (\alpha^*_{zz})_\sigma \tag{11}$$

and we can define a longitudinal effective thermal conductivity by the relation

$$K^*_{zz} = (\alpha^*_{zz})\langle\rho\rangle C_p \tag{12}$$

where

$$\langle\rho\rangle C_\rho = \epsilon_\beta(\rho c_p)_\beta + \epsilon_\sigma(\rho c_p)_\sigma. \tag{13}$$

The effective thermal conductivity K^*_{zz} has three contributions, one from conduction, one from hydrodynamic dispersion, and one from the heat exchange between fluid and solid. In the previous paper it was argued that one can estimate these three contributions using the results of previous experiments on the effective conductivity of stagnant beds (Nozad, 1983), the longitudinal dispersivity found from mass transfer experiments (Eidsath et al., 1983), and the effective diffusivity in packed beds (Ryan et al. 1981)

$$\frac{K^*_{zz}}{k_\beta} \simeq \frac{K_{\text{eff}}}{k_\beta} + \epsilon_\beta\left[\frac{D^*_{zz}}{\mathcal{D}} - \frac{D_{\text{eff}}}{\epsilon_\beta\mathcal{D}}\right] + \epsilon_\sigma Pe_p\left(\frac{\Delta}{d_p}\right)\left(\frac{K}{1+K}\right) \tag{14}$$

The capillary tube model results of Zanotti and Carbonell (1983) indicate that the hydrodynamic dispersion estimates from mass transfer measurements should overestimate this contribution, since the process of heat exchange between phases lowers hydrodynamic dispersion coefficients.

Lateral Effective Thermal Conductivity

Under steady state conditions the lateral effective thermal conductivity would have contributions from both pure heat conduction and hydrodynamic dispersion. The transport equation for the average bed temperature is

$$\langle v_\beta\rangle^\beta\cdot\nabla\langle T\rangle = \underset{\sim}{\alpha}^*:\nabla\nabla\langle T\rangle \tag{15}$$

where $\underset{\sim}{\alpha}^*$ is now the steady state effective thermal dispersivity for the packed bed. The lateral effective thermal conductivity can be obtained from the component normal to the flow direction

$$K^*_{yy} = (\alpha^*_{yy})\epsilon_\beta(\rho c_p)_\beta. \tag{16}$$

The terms contributing to K^*_{yy} can again be estimated from conductivities for the packed bed under no-flow conditions and from lateral dispersivities from mass transfer experiments in packed beds (Han et al. 1985)

$$\frac{K^*_{yy}}{k_\beta} = \frac{K_{\text{eff}}}{k_\beta} + \epsilon_\beta\left[\frac{D^*_{yy}}{\mathcal{D}} - \frac{D_{\text{eff}}}{\epsilon_\beta\mathcal{D}}\right]. \tag{17}$$

For details regarding the derivations and analysis leading up to these results the reader is referred to Part I. In this paper, we will be comparing the experimental results to Eqs. 3, 5, 14 and 17.

EXPERIMENTAL

An overall schematic diagram of the apparatus used is shown in Figure 1. A column 106 cm long with an inner square cross section 21 cm × 21 cm was constructed of 1.27 cm thick Plexiglas plates. The packing material consisted of urea formaldehyde spheres (0.55 cm and 0.25 cm dia.) which were supported by a stainless steel screen mounted 16.5 cm above the bottom of the column. Below the screen, an outlet distributor consisting of glued PVC tubes of 1.91 cm OD provided straight streamlines for the flow at the exit of the column. Flow rates were measured using high precision rotameters. The fluid (water) was pumped using 1 HP (0.746 kW) centrifugal pumps, and the water was heated using an immersion heater inserted into a 50 gal. (189 L) plastic drum. The column was designed so that both the longitudinal and lateral effective thermal conductivity measurements could be carried out with a minimum of modification of the appartus. At the same time it was necessary to ensure good flow uniformity across the column cross section and a sharp step disturbance in fluid temperature at the top of the bed. Since we were interested in measuring the temperature response of the solid particle as well as the fluid, it was necessary to design a special thermocouple bank for this purpose. We also had to design a thermocouple arrangement to measure temperature profiles perpendicular to the flow direction for the lateral effective conductivity measurements. Some of the details of construction of the more unusual items are given below.

Flow Distributor

The flow distributor had to serve two purposes. First, it had to provide a uniform flow distribution across the column; second, it had to allow a step change in fluid temperature to be introduced into the column with as sharp a front as possible. In order to meet both goals, it was constructed as a high-efficiency heat exchanger. It consists of two parallel brass plates (1.0 mm thick) perforated with 765 holes at 0.794 cm pitch. Stainless steel capillaries of 0.7 mm ID and 19 mm length were inserted in the holes so

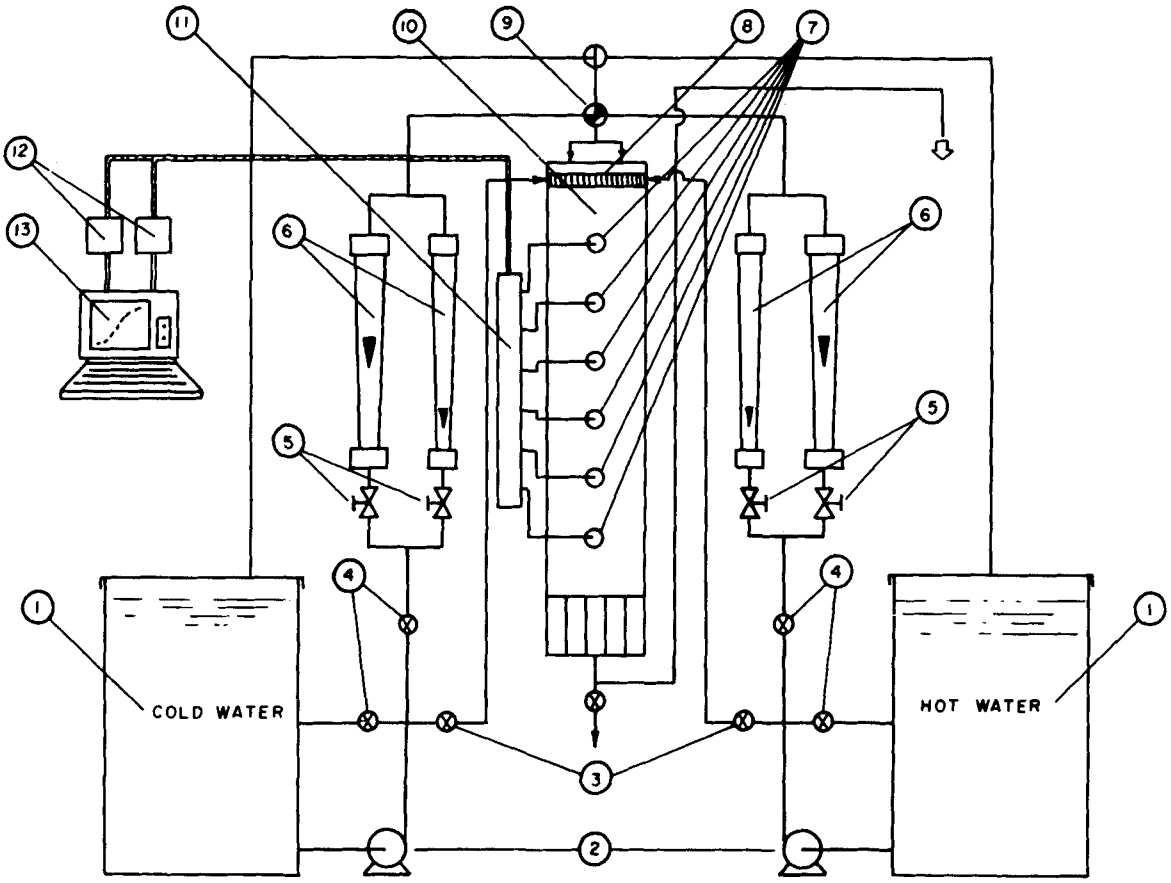

Figure 1. Diagram of apparatus.

1. Cold/hot water reservoirs
2. Centrifugal pumps
3. Heat exchanger valves
4. Bypass and input valves
5. Rotameter valves
6. Rotameters
7. Thermocouple banks
8. Distributor
9. Four-way valve
10. Packed bed
11. Amplifiers
12. Analog/digital converters
13. Computer

that the two plates were separated by the perpendicular capillary tubes. The tubes were pressed and soldered so that the distance between plates

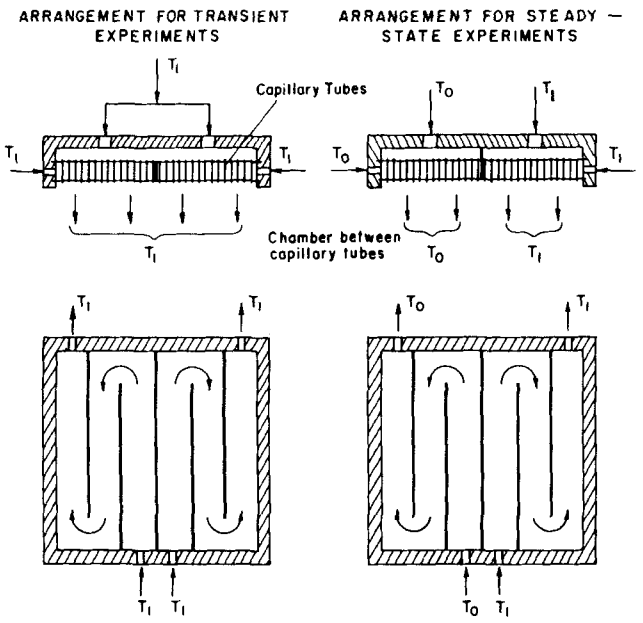

Figure 2. Flow distributor and heat exchanger.

was 12.7 mm. The space between the plates was divided in half by a 0.32 cm thick rubber divider, and baffles were added as shown in Figure 2. The inner dimensions of the distributor are the same as those of the column (21 cm × 21 cm). A perforated Plexiglas plate 0.32 cm thick was attached to the bottom brass plate to act as an insulator. The volume above the upper plate available for fluid is 320 cm^3. The stainless steel capillaries provided a sufficient pressure drop to insure flow uniformity, and the space between the plates allowed the system to be used as a heat exchanger. For the step temperature input in the transient experiments, water at a temperature T_1 was pumped through the space between the brass plates. This is the same temperature as the fluid coming into the column through the capillaries. This prevented heat losses in the incoming fluid and resulted in sharp step inputs. For the lateral effective thermal conductivity experiments the upper chamber was separated by a thin Plexiglas divider. One half of the distributor fluid was inserted at a temperature T_1, the other half at a lower temperature T_o. Typically, T_1 was around 50°C and T_o was around 20°C. This way a 30°C temperature gradient was maintained over a very short distance (6 mm or less) at the center of the bed.

Thermocouple Probes

In the transient step input experiments we wanted to measure the response of the fluid and the solid phases independently at various axial locations. The measurement of a fluid temperature in a packed bed is relatively simple if one insures that the thermocouple does not come in contact with any of the particles. The measurement of an average solid phase temperature is not as simple. We decided to approximate an average solid phase temperature at a given axial position in the bed by measuring the temperature at the center of a particle and at the surface of a particle. These surface and centerline temperatures were measured at the same axial position at which the fluid phase temperature was measured. In order to do this in a reproducible fashion, the thermocouple probe shown in Figure

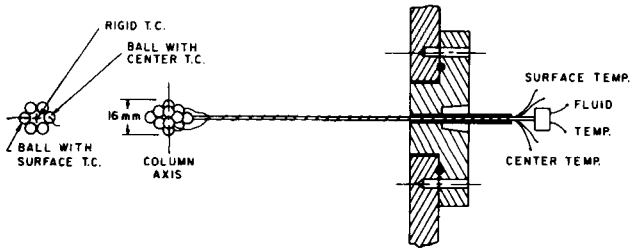

Figure 3. Probe to measure transient fluid and solid temperature responses in packed bed.

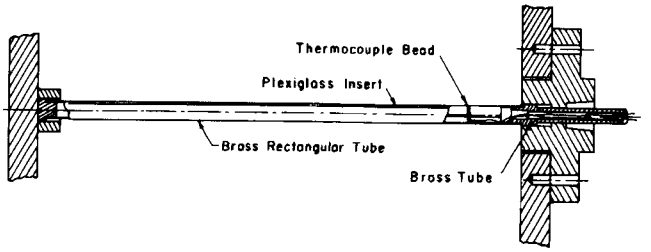

Figure 4. Probe to measure lateral temperature profiles.

3 was designed. Fourteen urea formaldehyde spheres 0.55 cm dia. were glued into a hexahedral aggregate, but with the sphere at the center omitted. A rigid thermocouple (J-type, 0.0508 cm dia., sheathed and grounded) was inserted through the sphere positioned at the apex of the hexahedron. The tip of this rigid thermocouple was positioned at the geometric center of the aggregate; it did not come in contact with any of the solid particles. This thermocouple measured the fluid phase temperature. Two of the particles in the aggregate lying in the same plane with the tip of the rigid thermocouple were used to measure surface and centerline temperatures. One sphere was drilled to the center, the other sphere was drilled completely through along its axis. Teflon-covered fine-gauge thermocouple wire (E-type, 0.0127 cm dia.) was used for the thermocouple inserted and cemented into the center of the first sphere. The same type of thermocouple wire was pushed through the hole in the second sphere until the thermocouple bead rested on the surface of the sphere; it was then cemented in place. Six of these thermocouple probes consisting of sphere aggregates were made and inserted into the column at six different axial positions: 12.7 cm, 25.4 cm, 38.1 cm, 50.8 cm, 63.5 cm, and 76.2 cm. We will refer to these as probes 1 through 6, respectively. Since the whole assemblage was supported by rigid thermocouples it was possible to determine very accurately the axial position of the thermocouples in the ensemble. The tip of the rigid thermocouple was always placed at the axis of the bed. The particles with surface and centerline thermocouples were always placed at the same axial position as the rigid thermocouple. Thermcouple response was investigated in preliminary tests. The slowest thermcouples were the larger J-type with a response time of less than 1 s. The fastest experiments that were performed involved a step duration of approximately 10 s. As a result, the error suspected due to intrinsic time lags in the thermocouples is very small. In addition to the six thermocouple assemblages, two fine-gauge thermocouples were placed below the bottom distributor plate in order to detect the arrival of the step input in temperature and to check its uniformity.

The temperature probes used to measure lateral temperature profiles in the steady state experiments are shown in Figure 4. Fourteen thermocouples made of Teflon-covered fine-gauge thermocouple wire (E-type, 0.0127 cm dia.) were inserted with equal 0.953 cm spacing into holes drilled in a Plexiglas bar with a rectangular cross section of 0.794 cm × 0.318 cm. The thermocouples were inserted through the holes from the bottom and cemented so that the thermocouple beads lay on the plane of the upper surface of the rod. The thermocouple wires were led to the outside of the column through a groove at the bottom of the Plexiglas bar. The entire bar was inserted into a brass rectangular tube to maintain rigidity. This brass tube was soldered to a cylindrical brass tube which served to lead the thermocouple wires to the outside of the column. The cylindrical brass tube assembly had two stop positions which allowed the entire probe to be displaced half the distance of the thermocouple separation (½ of 0.953 cm). This way, using 14 thermocouples one could get 28 temperature readings in the temperature profile by simply moving the assembly from one stop position to the other. Two of these probes were made; they could be placed at any of the six axial locations in the column that were used in the transient experiments.

Data Processing System

In the transient experiments, temperature vs. time data were collected at a total of 20 thermocouples. These consisted of three thermocouples for each of the six probes and two thermocouples placed below the bottom distributor plate in order to detect the step change in temperature at the inlet. The mV signals from the thermocouples passed through a bank of 100× signal amplifiers and then to two AI13 analog-to-digital converters (10 channels each) made by Interactive Structures, Inc. The digital signals were stored on disc by an Apple II computer. The data recording program was written in Basic with the time increment between readings controlled by a "do" loop. In the steady state experiments 16 thermocouple readings were taken at a time (14 from the thermocouple probes, two from below the distributor). For these experiments the thermocouples were connected directly to a 16-channel digital recorder.

Properties of the Packing

The urea formaldehyde particles used have the following physical properties: density $\rho_\sigma = 1.463$ g/cm^3, heat capacity $c_{p\sigma} = 0.4$ cal/g·K(1.7J/kg·K), thermal conductivity $k_\sigma = 2.5 \times 10^{-3}$ cal/s·cm·K. In the transient step input experiments, 0.55 cm dia. particles were used almost exclusively (except for two runs). In the steady state experiments for lateral measurements, both 0.55 cm and 0.25 cm dia. spheres were employed. Bed porosities were obtained by carefully weighing the particles prior to packing them into the column. Air bubbles were prevented by degassing the water and packing the bed while filled with water. Approximately 4 cm of packing was added at a time; it was carefully patted down so that the packing would be as uniform as possible. The volume fractions of fluid obtained were very close to a value of $\epsilon_\beta = 0.4$.

Procedure

In almost all runs the hot water was maintained at about 50°C (T_1) while the cold water was at room temperature, near 20°C (T_o). A step change in temperature in the bed was obtained by first bringing the bed to an initial temperature T_o by pumping water at the desired flow rate. Meanwhile the hot water (T_1) was adjusted to the same flow rate while bypassing the column. The position of the four-way valve (⑨) shown in Figure 1 was quickly changed, and shortly after, ball-valve (③) was fully opened. This simultaneously changed the fluid in the distributor and the heat exchanger from temperature T_o to T_1. We found that there was very little loss of thermal energy to the outside of the column during the course of an experiment due to the low thermal diffusivity of the Plexiglas walls. Temperature measurements as a function of time in the fluid and solid were collected at the known axial locations. In the steady state experiments one side of the distributor and heat exchanger was fed hot water (T_1) while the other side was fed cold water (T_o). The spread of the temperature profile in the direction perpendicular to flow was measured at least at two axial positions when steady state conditions were reached. Every time the lateral temperature probes were moved from one stop position to another, the system was allowed to reach steady state prior to taking measurements. The viscosity of the hot fluid was increased with small amounts (~0.5 wt%) of CMC (carboxymethylcellulose) in order to offset the variation of fluid viscosity with temperature. To test for possible fingering effects due to an unfavorable viscosity gradient, some transient experiments were done by replacing hot fluid with cold fluid. No differences in behavior, qualitative or quantitative, were found.

ANALYSIS OF EXPERIMENTAL DATA

Longitudinal Effective Thermal Conductivity

From measurements of the fluid temperature and the solid phase temperature as a function of axial position z and time t, we can use Eqs. 1 and 2 to calculate values of the pulse velocities u_β and u_σ and the longitudinal effective thermal conductivities $(\alpha^*_{zz})_\beta$ and $(\alpha^*_{zz})_\sigma$. We can rewrite these equations in the general form

$$\frac{\partial \langle T_\omega \rangle^\omega}{\partial t} + u\omega \frac{\partial \langle T_\omega \rangle^\omega}{\partial z} = (\alpha^*_{zz})_\omega \frac{\partial^2 \langle T_\omega \rangle^\omega}{\partial z^2} \qquad (18)$$

where ω can apply to either the fluid or the solid phase, $\omega = \beta, \sigma$. We know these equations should apply for distances into the bed which are of the order (Levec and Carbonell, 1985)

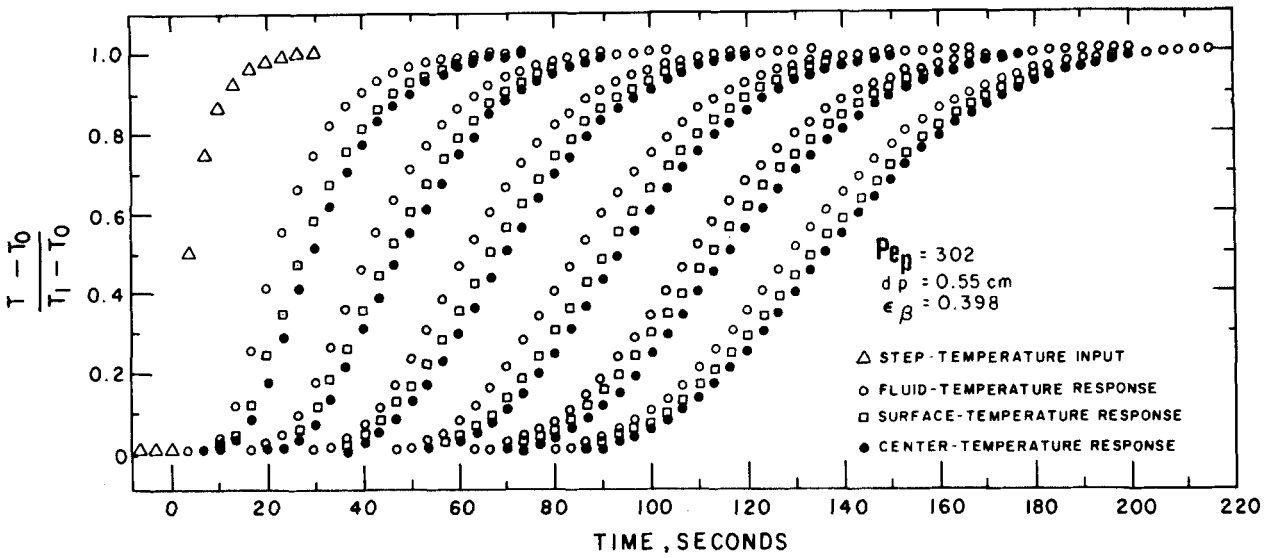

Figure 5. Sample response of packed bed to step-temperature input at inlet.

$$z \geq \frac{1}{6}\frac{Pe_p}{Nu}\frac{K}{(1+K)^2}d_p \tag{19}$$

If these distances are not too large, we can solve Eq. 18 with boundary conditions at $z = \infty$ with little error, so that we can apply the initial and boundary conditions

$$\begin{aligned} \langle T_\omega\rangle^\omega &= T_0 \quad t = 0 \quad \text{for all } z \\ \langle T_\omega\rangle^\omega &= T_1 \quad z = 0 \quad t > 0 \\ \langle T_\omega\rangle^\omega &= T_0 \quad z = \infty \quad t > 0. \end{aligned} \tag{20}$$

for $\omega = \beta, \sigma$.

The solution to Eq. 18 then takes the form

$$\frac{\langle T_\omega\rangle^\omega - T_o}{T_1 - T_o} = \frac{1}{2}\left\{\operatorname{erfc}\left(\frac{z - u_\omega t}{\sqrt{4(\alpha^*_{zz})_\omega t}}\right) + \exp\left[\frac{zu_\omega}{(\alpha^*_{zz})_\omega}\right]\operatorname{erfc}\left(\frac{z + u_\omega t}{\sqrt{4(\alpha^*_{zz})_\omega t}}\right)\right\}. \tag{21}$$

From a knowledge of $\langle T_\beta\rangle^\beta$ and $\langle T_\sigma\rangle^\sigma$ vs. time at each z, we can use a search routine to find the optimal values of u_σ, u_β, $(\alpha^*_{zz})_\beta$, and $(\alpha^*_{zz})_\sigma$ which satisfy this equation. Of course, in the case of the solid phase temperature measurements the raw data consist of a surface temperature T_s and a centerline temperature T_c. In Appendix A we show that a very good approximation for the average temperature of the solid can be obtained from these two values

$$\langle T_\sigma\rangle^\sigma \simeq T_s\left(1 - \frac{3}{\pi^2}\right) + T_c\left(\frac{3}{\pi^2}\right). \tag{22}$$

This expression weights the surface temperature by a factor of about 0.7 and the center temperature by a factor of about 0.3 for spherical particles. Once the thermal dispersivities are calculated, one can compute the longitudinal effective thermal conductivity by using Eq. 12 with the known values of the density and heat capacity for the fluid and solid.

Lateral Effective Thermal Conductivity

In the steady state experiments described in the previous section, a steep temperature gradient is imposed at the bed entrance ($z = 0$) along the y direction. The temperature is uniform along the x direction, and the gradients remain much steeper along y than along the flow direction throughout the entire length of the column. One can then write Eq. 15 in the form

$$\langle v_\beta\rangle^\beta \frac{\partial\langle T\rangle}{\partial z} = \alpha^*_{yy}\frac{\partial^2\langle T\rangle}{\partial y^2}, \tag{23}$$

subject to the approximate boundary conditions

$$\langle T\rangle = \begin{cases} T_1 & 0 < y < \infty,\ z = 0 \\ T_0 & -\infty < y < 0 \end{cases} \tag{24}$$

$$\langle T\rangle = T_1 \qquad y \to \infty \tag{25}$$

$$\langle T\rangle = T_o \qquad y \to -\infty. \tag{26}$$

The solution to Eq. 23 is of the form

$$\frac{\langle T\rangle - T_o}{T_1 - T_o} = \frac{1}{2}\operatorname{erfc}\left(\frac{y}{\sqrt{\frac{4(\alpha^*_{yy})z}{\langle v_\beta\rangle^\beta}}}\right) \tag{27}$$

By direct measurements of $\langle T\rangle$ as a function of y at various axial locations, it is possible to calculate the lateral component of the thermal dispersivity α^*_{yy} using Eq. 27. The lateral effective thermal conductivity is then computed using Eq. 16.

RESULTS AND DISCUSSION

Longitudinal Effective Thermal Conductivity

In Figure 5 we show a typical set of step response curves at the six axial locations of the thermocouple assemblies (z = 12.7 cm, 25.4 cm, 38.1 cm, 58.8 cm, 63.5 cm, and 76.2 cm). Note that at a fixed instant of time the temperature of the fluid phase is greater than that at the particle surface, which in turn is larger than the temperature at the center of the particle. For Peclet numbers greater than 20 it was not difficult to resolve the difference between fluid and solid temperatures. In Figure 5 we also show the response of the thermocouple immediately below the lower distributor plate, indicating a fairly sharp step input. At higher Peclet numbers the input response was even closer to a perfect unit step. Some step response experiments were carried out by lowering the inlet temperature. However, we observed some fingering and flow instabilities at low Peclet numbers in this mode of operation primarily due to the unstable configuration of a high-density fluid above one of lower density. As we will see later, when the Peclet numbers were high enough and these natural convection instabilities were not a problem, the lateral effective thermal conductivities were independent of the type of disturbance. From the measured surface and center temperature response of the particles one can compute the response of the average solid phase temperature using Eq. 22. The pulse velocities u_β and u_σ and the longitudinal dispersivities $(\alpha^*_{zz})_\beta$ and $(\alpha^*_{zz})_\sigma$ can be calculated by applying Eq. 21 to the fluid phase temperature response $\langle T_\beta\rangle^\beta(t)$ and the solid phase temperature response $\langle T_\sigma\rangle^\sigma(t)$ at each of the six axial locations z of

TABLE 1. PARAMETERS USED IN THE DATA ANALYSIS

Physical Properties of Fluid and Solid		
Solid (urea formaldehyde)	$\rho_\sigma = 1.463$ g/cm^3	
	$c_{p\sigma} = 0.4$ cal/g·K	
	$k_\sigma = 2.50 \times 10^{-3}$ cal/c·s·K	
	$\alpha_\sigma = 4.32 \times 10^{-3}$ cm^2/s	
Fluid (water, 37°C)	$\rho_\beta = 0.993$ g/cm^3	
	$c_{p\beta} = 0.9987$ cal/g·K	
	$k_\beta = 1.469 \times 10^{-3}$ cal/s·c·/K	
	$\alpha_\beta = 1.48 \times 10^{-3}$ cm^2/s	
Conductivity ratio	$\kappa = 1.70$.	
Void fractions (two packings)	$\epsilon_\beta = 0.398$	$\epsilon_\beta = 0.390$
Ratio of heat capacities K	0.885	0.923
Overall heat capacity $\langle\rho\rangle C_p$ (Cal/cm^3·K)	0.748	0.744
Pe_p range	10–10^3	
Particle diameters	$d_p = 0.55$ cm; $d_p = 0.25$ cm	

Probe locations:	Probe #:	1	2	3	4	5	6
	z (cm):	12.7	25.4	38.1	50.8	63.5	76.2

SI conversion: J = cal × 4.1868.

measurement. This results in pulse velocities and longitudinal dispersivities for each axial position. One can then see how the parameters in Eqs. 1 and 2 vary with location in the bed.

Equation 19 can be used to predict the distance into the bed for which u_β, u_σ, $(\alpha^*_{zz})_\beta$ and $(\alpha^*_{zz})_\sigma$ should be independent of axial location. In Table 1 we list some of the values of the physical and bed parameters used in the computations of the transport coefficients. If we use Eq. 19 to calculate the distance z at which we expect the transport parameters to be constant, we find for the highest Peclet numbers $Pe_p = 10^3$, and the largest particles $d_p = 0.55$ cm, that $z \geq 3$ cm. Here we used the correlation of Schlünder (1978) to compute Nu_f in Eq. 6. This means that we should find the pulse velocities and longitudinal dispersivities to be essentially independent of axial position throughout the entire range of the experiments, and this was indeed the case. The values obtained for u_β were only slightly smaller at $z = 12.7$ cm than those measured at the other probe locations (by about 5%). In Figure 6 we show the ratio of the pulse velocity in the fluid phase u_β to the interstitial average velocity $\langle v_\beta\rangle^\beta$ as a function of Pe_p. These are the averages of the pulse velocities measured at all the probe locations, but as mentioned above there is no more than a 5% variation between them. According to Eq. 3, this ratio of $u_\beta/\langle v_\beta\rangle^\beta$ should be independent of Pe_p and should take on the value $1/(1 + K)$. Since K is known from the physical properties in Table 1, this serves as a good test of the accuracy of the pulse velocity data. In Figure 6 we see the data points compared to the theoretically predicted value of $u_\beta/\langle v_\beta\rangle^\beta = 0.503$. We find that the experimentally determined ratio $u_\beta/\langle v_\beta\rangle^\beta$ is independent of Peclet number and is very close in magnitude to the predicted value.

The solid phase pulse velocities u_σ were found to be a little more dependent on axial location in the bed than the u_β, especially at the high Peclet numbers. The pulse velocity u_σ measured at the first thermocouple probe location ($z = 12.7$ cm) was about 10% lower than the final value at the last probe location ($z = 76.2$ cm). In Figure 7 we show the ratio of u_β to u_σ as a function of Peclet number. According to Eq. 3 this ratio should be 1 and independent of Pe_p. Clearly the data indicate very good agreement with this value, except perhaps at the largest Peclet numbers where the experimentally observed ratio is near 0.8. Part of the reason for this discrepancy at large Peclet numbers may be a slight sensitivity of the data to the time lag of the rigid thermocouples. As was mentioned previously, this could result in a measured response which is about 10% slower than it should be. This can account for smaller values of u_β at very high Peclet numbers.

The theory also predicts that when Eq. 3 is satisfied, the longitudinal dispersivities for the fluid and solid should be identical, as indicated in Eq. 11. The values of $(\alpha^*_{zz})_\beta$ and $(\alpha^*_{zz})_\sigma$ were found to be much smaller at the first probe than in subsequent probe locations, especially at high Peclet numbers. For example, when $Pe_p = 1{,}174$, the value of $(\alpha^*_{zz})_\beta$ was 3.79 cm^2/s at $z = 12.7$ cm and 8.59 cm^2/s at $z = 76.2$ cm. However, for probes 4, 5, and 6 there was very little difference in the magnitudes of the measured dispersivities. In Figure 8 we show the ratio of $(\alpha^*_{zz})_\sigma$ to $(\alpha^*_{zz})_\beta$ as a function of Pe_p. These are the averages of the values found at probes 4, 5, and 6. Again the ratio is very close to 1, in agreement with Eq. 11, except at high Peclet numbers. The data for $(\alpha^*_{zz})_\sigma$ and $(\alpha^*_{zz})_\beta$ show some scatter in the values measured at different probes, the variations being on the order of 20% of the average values at the high Peclet numbers. If we take the measured values of $(\alpha^*_{zz})_\beta$ at several probe locations and multiply by the average bed heat capacity as shown in Eq. 12, we get the results for longitudinal effective thermal conductivity shown in Figure 9. These data provide a good idea of the trends and scatter in the longitudinal effective thermal conductivities, even though they do not include all the measurements taken. Throughout the entire range of Pe_p they are nearly constant with axial position in the bed after probe 4.

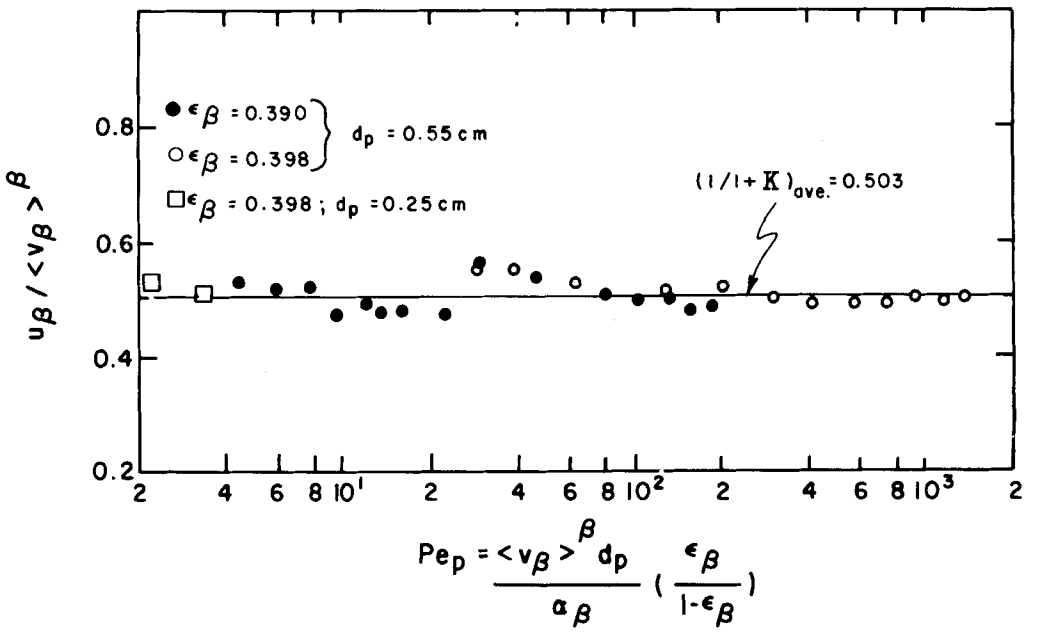

Figure 6. Velocity of temperature disturbance in fluid phase.

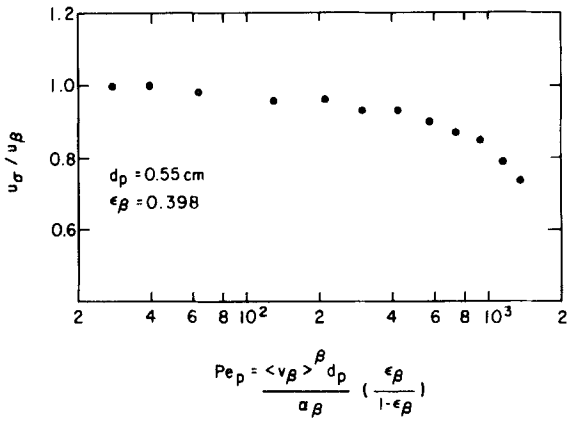

Figure 7. Ratio of velocity of disturbance in solid and fluid phases.

From the type of time response curves shown in Figure 5 we can also measure values of the spatial pulse separation Δ between the fluid and solid temperature fields. We can do this by first defining the dimensionless temperature change for the response of the ω phase as

$$\theta_\omega = \frac{\langle T_\omega \rangle^\omega - T_o}{T_1 - T_o}, \qquad \omega = \sigma, \beta.$$

The mean residence time for the disturbance in the fluid and the solid can be defined as the time at which $\theta_\omega = 1/2$ at each axial position so that

$$\bar{t}_\sigma \equiv \text{Time at which } \theta_\sigma = 1/2$$
$$\bar{t}_\beta \equiv \text{Time at which } \theta_\beta = 1/2.$$

The separation between fluid phase and solid phase breakthrough curves can then be computed using the values of the pulse velocities

$$\Delta = u_\sigma \bar{t}_\sigma - u_\beta \bar{t}_\beta \tag{28}$$

Of course, since $u_\beta \cong u_\sigma$ for the entire range of Peclet numbers in this experiment, the separation Δ really only depends on the difference in mean residence times.

In Figure 10 we show the results for the separation Δ/d_p as a function of Peclet number. At Peclet numbers around 10^3 the distance between the fluid and solid temperature response curves corresponds to about 20 particle diameters. Since the temperature gradients in the column are so steep, this means that there is a very large difference between the average temperature of the fluid and that of the solid. In Figure 10 we have also included a theoretical curve based on the predictions of Eq. 5 with $S_{\beta\beta} + S_{\beta\sigma} = 0$

$$\frac{\Delta}{d_p} = \frac{1}{6}\frac{Pe_p}{Nu}\left(\frac{K}{1+K}\right). \tag{29}$$

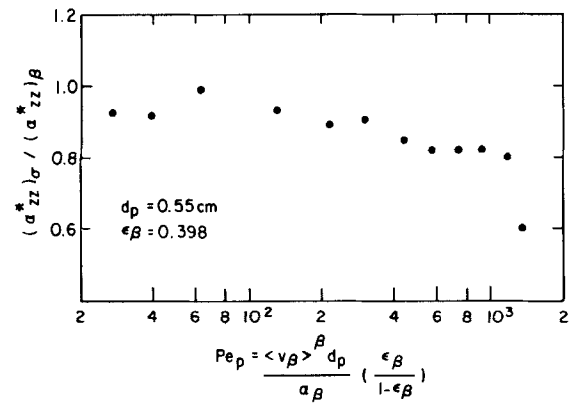

Figure 8. Ratio of longitudinal thermal dispersivity in solid and fluid phases.

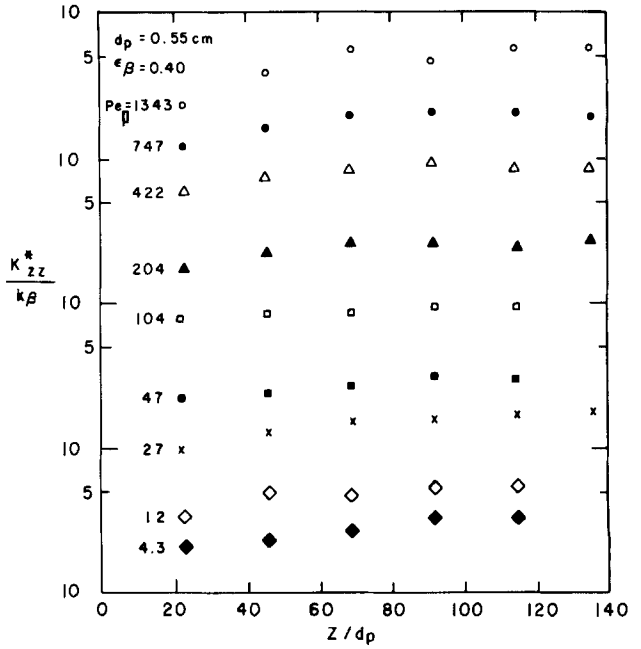

Figure 9. Longitudinal effective thermal conductivities measured at various probe locations for several Peclet numbers.

The value of the Nusselt number based on the film heat transfer coefficient, Nu_f in Eq. 6, was computed using the correlation of Schlünder (1978). The correlation of Whitaker (1972) was also used with nearly identical results. Values of K and κ in Eq. 6 are given in Table 1. As can be seen in Figure 10, Eq. 29 underestimates the value of Δ/d_p by a factor of 3 at low Peclet numbers and a factor of 2 at $Pe_p = 10^3$. The error of a factor of 2 at high Peclet numbers is very significant since the gradients of the temperature field are extremely steep. Equation 29 would predict that the fluid and solid temperatures are much closer in value than they are in fact. As was pointed out previously, Eq. 29 is the prediction of the pulse separation that one obtains using the dispersion concentric heat transfer model (Sáez and McCoy, 1982) and the continuous solid phase model (Vortmeyer and Berninger, 1982). Clearly, the contributions to Δ/d_p arising from the additional cross-coupling terms in the new heat transfer model developed by Levec and Carbonell (1985) are not insignificant. In order for the experimental results shown in Figure 10 to match the theoretical prediction in Eq. 5, the cross-coupling contribution should take on the value

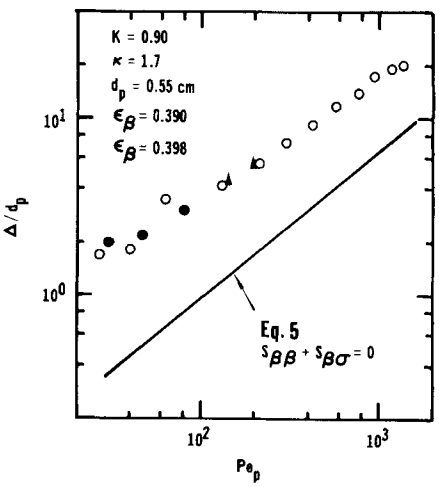

Figure 10. Separation between mean position of temperature disturbance in fluid and solid phases as a function of Peclet number. ▲: experiments in which hot fluid replaced cold fluid.

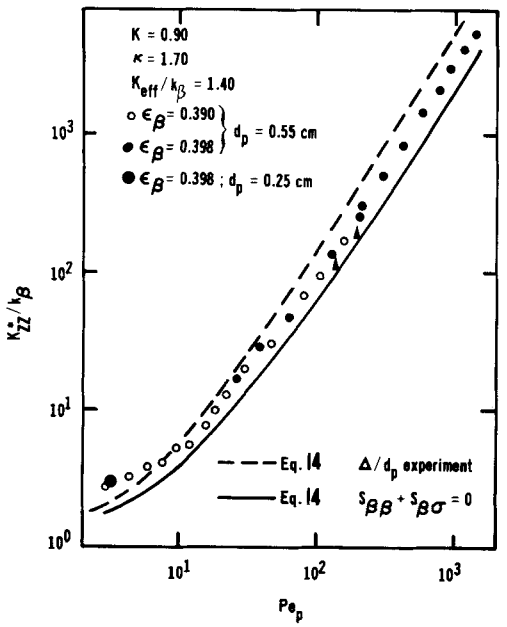

Figure 11. Longitudinal effective thermal conductivity as a function of Peclet number. ▲: experiments in which hot fluid replaced cold fluid.

$$-\frac{(S_{\beta\beta} + S_{\beta\sigma})}{Nu} = (0.299)Pe_p^{0.569}\left(\frac{\epsilon_\beta}{\epsilon_\sigma}\right). \qquad (30)$$

The prediction from the capillary tube model in Eq. 7 is of the same order of magnitude as Eq. 30; however, it has a much stronger Peclet number dependence and it is in serious discrepancy with experimental observations at low Peclet numbers.

In Figure 11 we have plotted the average values of K^*_{zz}/k_β measured at probes 4, 5, and 6 as a function of Peclet number for all of the experiments. This represents our final summary of the observed longitudinal effective thermal conductivities in the packed bed under flow conditions. In Figure 11 we have also plotted two theory lines, based on the estimates of the various contributions to the longitudinal effective thermal conductivity shown in Eq. 14. For both theory lines we used the effective thermal conductivity under no-flow conditions for a packed bed with $\kappa = 1.70$ and $\epsilon_\beta = 0.40$ as correlated by Nozad (1983)

$$\frac{K_{eff}}{k_\beta} = 1.40 \qquad (\kappa = 1.70, \quad \epsilon_\beta = 0.40). \qquad (31)$$

The value used for the effective diffusivity of the packed bed under the same conditions was taken from the work of Ryan et al. (1981)

$$\frac{D_{eff}}{\epsilon_\beta \mathcal{D}} = 0.70 \qquad (\epsilon_\beta = 0.40). \qquad (32)$$

The longitudinal dispersivity data from mass transfer experiments as reported by Han et al. (1985) was correlated by the empirical equation

$$\frac{D^*_{zz}}{\mathcal{D}} = 0.357\, Pe_p^{1.256} \qquad 10 < Pe_p < 10^3. \qquad (33)$$

The two theory lines shown in Figure 11 correspond to the use of two different values for Δ/d_p in order to estimate the contribution from heat exchange between phases. In the upper curve we have used the experimental Δ/d_p values from Figure 10, and as can be seen, we overestimate the value of K^*_{zz} by a small amount. One reason for this could be that Eq. 33 probably overestimates the hydrodynamic dispersion contribution. In the capillary tube analysis of Zanotti and Carbonell (1984) the heat exchange process taking place between the fluid and the solid phases tended to lower the magnitude of the hydrodynamic dispersion term. The same thing might be happening in the packed bed observations.

In the lower curve of Figure 11 we have used the Δ/d_p values

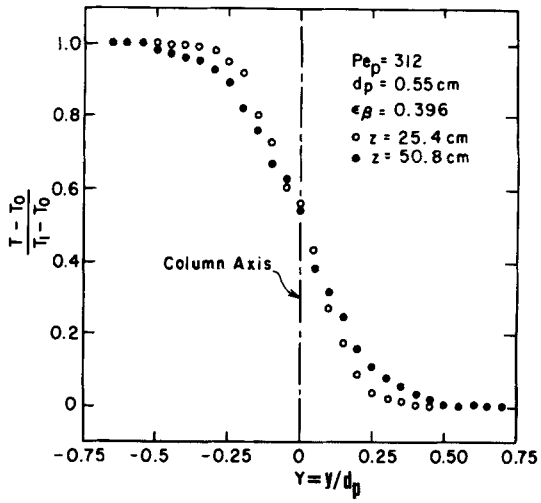

Figure 12. Sample temperature profiles at two axial locations in experiment to measure lateral effective thermal conductivity.

calculated from Eq. 29. This is the Δ/d_p value predicted from the more traditional heat transfer models. The agreement is not bad in this case either, but the calculated values of the effective thermal conductivity fall below the experimental results. At Peclet numbers above 500 the heat exchange term in Eq. 14 tends to dominate the value of the longitudinal effective thermal conductivity. For example, at $Pe_p = 1{,}500$, the ratio of the heat exchange term to the hydrodynamic dispersion term is approximately 10. In arriving at Eq. 14, we neglected completely some additional dispersive terms that affected the heat transfer contributions to K^*_{zz}/k_β. These were the terms D_β and τ_β in Eq. 65 of the preceding paper. We were able to determine that D_β and τ_β have a magnitude that is bound between 0 and 1, but we cannot say anything a priori about their sign. The top theoretical line in Figure 11 should be the most accurate since it relies on experimental Δ/d_p data. This indicates that these additional terms could be negative and lead to a reduction in the magnitude of the predicted values of K^*_{zz}/k_β.

Lateral Effective Conductivity

In Figure 12 we show a typical steady state temperature profile measured along the direction perpendicular to flow at two different axial locations in the packed bed. Note that the temperature gradients are very narrow, and that the center of the bed ($Y = 0$) corresponds closely to the point where the dimensionless temperature is 0.5. Furthermore, the measured dimensionless temperature approaches a value of 1 and 0 at either side of the column, so that there are no significant heat loss effects from the sides of the bed. These observations justify the use of Eq. 27 to calculate α^*_{yy} from measured values of $(\langle T\rangle - T_o)/(T_1 - T_o)$ as a function of y for one or two axial locations z. By plotting the inverse complementary error function of the unaccomplished temperature as a function of y, one can compute α^*_{yy} from the slope. The lateral effective thermal conductivity is then calculated using Eq. 16 with the values of heat capacity shown in Table 1. The results are summarized in Figure 13 for a Peclet number range from 10 to 10^3. In Figure 13 we also show the predictions of Eq. 17 with the effective conductivity under no-flow conditions taken from Eq. 31, the effective diffusivity from Eq. 32, and the lateral dispersivities from mass transfer experiments correlated by Han et al. (1985)

$$\frac{D^*_{yy}}{\mathcal{D}} = 0.39\, Pe_p^{0.683} \qquad 10 < Pe_p < 10^3. \qquad (34)$$

Even though the predictions of K^*_{yy} using Eq. 17 are of the same order as those measured experimentally, and the agreement is fairly good at Peclet numbers from 10 to 10^2, there is a significant difference at high Peclet numbers with the experimental values nearly a factor of 3 higher than the theory at $Pe_p = 1{,}500$. There are two possible reasons for this. The first is that in Eq. 17 we neglect any

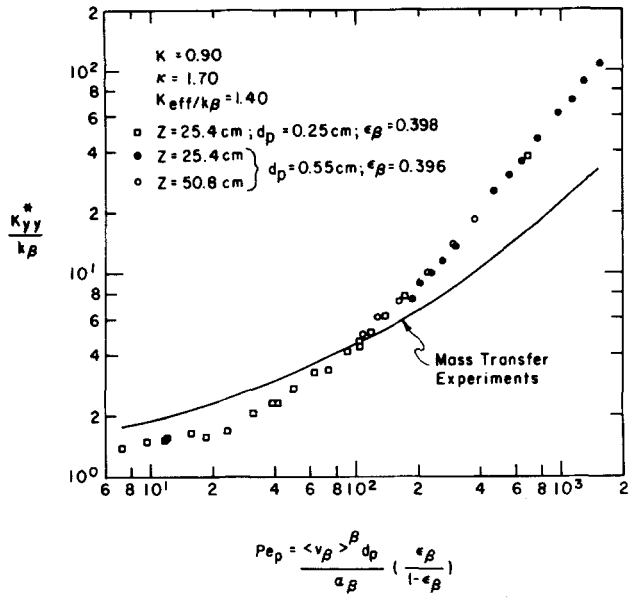

Figure 13. Lateral effective thermal conductivities as a function of Peclet number.

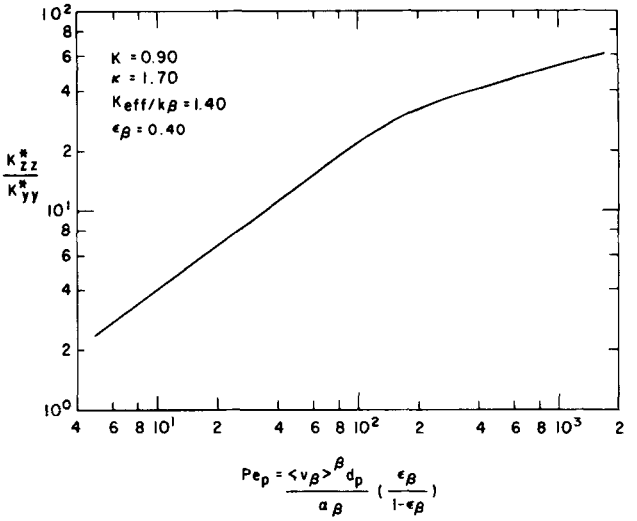

Figure 14. Ratio of longitudinal to lateral effective thermal conductivities as a function of Peclet numbers.

possible influence of particle conduction on the hydrodynamic dispersion contribution. One would think that the conductivity of the particles would have a strong enough influence on the temperature field in the fluid to cause an important change in the hydrodynamic dispersion coefficient from that found in mass transfer experiments. This influence is stronger at high Peclet numbers where the temperature gradients tend to be steeper at a fixed axial location. The second possible explanation for the observed difference between experimental values of K^*_{yy} and the values predicted by Eq. 17 is the influence of density and viscosity gradients on the local flow field. These experiments were done with water at 40°C to 50°C on one side of the bed and water at approximately 20°C on the other side of the bed. This difference in water temperature is enough to cause a difference in fluid viscosities of nearly a factor of two [μ(52°C) = 0.529 *cp*; μ(22°C) = 0.955 *cp*]. The fluid density difference at these two temperatures is small but not insignificant [ρ_β (52°C) = 0.984 g/cm^3; ρ_β (22°C) = 0.998 g/cm^3]. At low Peclet numbers this density difference was enough to cause significant natural convection in the column and temperature profiles that were shifted toward the cold fluid side of the bed. At large Peclet numbers the difference in the viscosities was enough to cause the hotter fluid to be able to move faster than the colder fluid (larger permeability) and this resulted in temperature profiles that were shifted toward the hot end of the bed. In order to ensure that all the temperature fields were centered at $Y = 0$, as the one shown in Figure 12, we adjusted the fluid viscosity by adding small amounts of carboxymethylcellulose (CMC) to the hot fluid. The amounts added were small enough (0.5% by weight) that the fluid was still Newtonian, but large enough to result in an increase in viscosity. By a proper choice of viscosity, the natural convection effect due to the density differences tending to make the cold fluid move faster was counterbalanced by the viscous effects tending to make the hot fluid move faster. In Figure 13 we have shown only lateral conductivities calculated from temperature profiles where $Y = 0$ was the point at which the unaccomplished temperature change is 0.5. Note that values at low Peclet numbers were obtained using smaller particle diameters to reduce the Grashoff number for natural convection. The difference between the theoretical K^*_{yy} calculated from Eq. 17 and the experimental K^*_{yy} values can then simply be due to the difference in the hydrodynamic flow field in the region where the temperature gradients exist. The mass transfer experiments are done under conditions where the fluid density and viscosity are identical (low tracer concentrations). The heat transfer experiments are done under conditions where the fluid viscosity and density must differ by necessity. Many previous measurements of lateral effective thermal conductivities were done by heating the surface of cylindrical packed beds (Gunn and Khalid, 1975; Kunii and Ono, 1968). This results in large viscosity and density differences between the fluid near the wall and that at the center of the bed. As a result, one can expect that lateral effective thermal conductivities taken under these conditions would be influenced significantly by the flow field generated from density and viscosity differences. One would expect that these measured conductivities should depend not only on local Reynolds and Prandtl numbers, but also on the temperature difference between the wall and the bulk fluid, since this is the quantity that determines density and viscosity differences.

It should also be mentioned that Dixon and Cresswell (1979) have reported mass transfer lateral dispersion measurements which have a Peclet member dependence that is nearly linear, instead of the dependence shown in the experiments of Han et al. (1985). The increased dependence on the Peclet number would make the agreement in Figure 13 much better.

In Figure 14 we have plotted the observed ratio of the longitudinal to lateral effective thermal conductivities. For very low Peclet numbers the longitudinal and lateral conductivities become nearly equal. However, at high Peclet numbers we find that this ratio can take extremely high values. The reason for this is that the longitudinal effective thermal conductivities are taken under transient conditions and the heat exchange term between phases dominates at high Peclet number. The lateral effective thermal conductivities are taken under steady state conditions where the fluid and solid temperatures are equal and there is no net heat exchange between phases. As a result, lateral conductivities increase with increasing Peclet number much more slowly than the longitudinal conductivities.

ACKNOWLEDGMENT

The authors wish to thank the Fulbright Foundation for a Fellowship given for the financial support of J. Levec during the course of this investigation. This work was sponsored by the National Science Foundation, under grant ENG 79-13269.

APPENDIX A

Consider a single spherical particle in the packed bed, initially at a uniform temperature T_o, subjected to a fluid temperature disturbance as the wave of hot fluid passes around the particle. We can approximate the temperature distribution inside the particle by solving the transient heat conduction equation subject to a time-dependent temperature on the particle surface. In dimensionless variables we can write

$$\frac{\partial\theta}{\partial\tau} = \frac{1}{\eta^2}\frac{\partial}{\partial\eta}\left(\eta^2\frac{\partial\theta}{\partial\eta}\right) \tag{A1}$$

with boundary and initial conditions

$$\theta = 0 \qquad \tau = 0 \tag{A2}$$

$$\theta = \theta_s(\tau)\ \eta = 1 \tag{A3}$$

$$\theta \text{ finite} \quad \eta = 0 \tag{A4}$$

Here τ is a dimensionless time

$$\tau = t\alpha_o/r_0^2, \tag{A5}$$

η is a dimensionless radial position

$$\eta = r/r_o, \tag{A6}$$

and θ is the unaccomplished temperature difference

$$\theta = \frac{T - T_o}{T_1 - T_o}\,. \tag{A7}$$

The quantity θ_s is the dimensionless temperature on the particle surface, which is assumed independent of position along the surface.

The solution to Eq. A1 subject to the initial and boundary conditions imposed is given by

$$\theta(\eta,\tau) = \frac{\partial}{\partial\tau}\int_o^\tau \theta_s(\tau-\lambda)\left\{1 + 2\sum_{n=1}^{\infty}(-1)^n\frac{\sin(n\pi\eta)}{n\pi\eta} \times \exp[-(n\pi)^2\lambda]\right\}d\lambda. \tag{A8}$$

The temperature at the center of the particle is obtained by letting $\eta = 0$

$$\theta_c = \frac{d}{d\tau}\int_o^\tau \theta_s(\tau-\lambda)\left\{1 + 2\sum_{n=1}^{\infty}(-1)^n\exp[-(n\pi)^2\lambda]\right\}d\lambda. \tag{A9}$$

The average temperature of the solid particle can be calculated by substituting Eq. A8 in the integral

$$\langle\theta\rangle = 3\int_o^1 \theta\eta^2 d\eta. \tag{A10}$$

This results in the expression

$$\langle\theta\rangle = \frac{d}{d\tau}\int_o^\tau \theta_s(\tau-\lambda)\left\{1 - 6\sum_{n=1}^{\infty}(n\pi)^{-2}\exp[-(n\pi)^2\lambda]\right\}d\lambda. \tag{A11}$$

The first term in Eqs. A9 and A11 can be greatly simplified by using the substitution $\xi = \tau - \lambda$ and the Leibnitz rule for differentiating an integral

$$\frac{d}{d\tau}\int_o^\tau \theta_s(\tau-\lambda)d\lambda = \frac{d}{d\tau}\int_o^\tau \theta_s(\xi)d\xi = \theta_s(\tau). \tag{A12}$$

Equations A9 and A11 can then be written in the form

$$\theta_c = \theta_s + 2\sum_{n=1}^{\infty}(-1)^n F_n(\tau) \tag{A13}$$

$$\langle\theta\rangle = \theta_s - 6\sum_{n=1}^{\infty}(n\pi)^{-2}F_n(\tau) \tag{A14}$$

where

$$F_n(\tau) = \frac{d}{d\tau}\int_o^\tau \theta_s(\tau-\lambda)\exp[-(n\pi)^2\lambda]d\lambda. \tag{A15}$$

From the form of Eq. A15 it is not difficult to see that the functions F_n are successively smaller for larger n values

$$F_1 < F_2 < F_3 \ldots \tag{A16}$$

Furthermore, for surface temperatures $\theta_s(\tau)$ which are monotonically increasing in τ and that eventually reach a constant value, the functions $F_n(\tau)$ tend to decrease exponentially with increasing τ. For example, if $\theta_s(\tau)$ is a unit step function in time, then

$$F_n(\tau) = \exp[-(n\pi)^2\tau]. \tag{A17}$$

As a result, we can consider time τ long enough that only the first term in the series in Eqs. A13 and A14 are necessary

$$\theta_c \simeq \theta_s - 2F_1(\tau) \tag{A18}$$

$$\langle\theta\rangle \simeq \theta_s - \frac{6}{\pi^2}F_1(\tau). \tag{A19}$$

Solving for F_1 in Eq. A18 and substituting the result in Eq. A19 we find

$$\langle\theta\rangle \simeq \theta_s\left(1 - \frac{3}{\pi^2}\right) + \theta_c\left(\frac{3}{\pi^2}\right). \tag{A20}$$

This way, from a knowledge of time-dependent surface temperatures and center temperatures for the particles, one can estimate the average particle temperature. Substituting the definition of the dimensionless temperature in Eq. A20 we obtain the final result

$$\langle T_\sigma\rangle^\sigma = T_s\left(1 - \frac{3}{\pi^2}\right) + T_c\left(\frac{3}{\pi^2}\right). \tag{A21}$$

Here we have associated the volume-averaged solid phase temperature with the average temperature of a single-particle.

NOTATION

$c_{p\omega}$ = heat capacity per unit mass of ω phase
C_p = heat capacity per unit mass of bed
d_p = particle diameter
$\mathcal{D}$ = molecular diffusivity
D_{eff} = effective diffusivity in packed bed
D^*_{zz}, D^*_{yy} = longitudinal and lateral dispersivities in packed bed
F_n = time-dependent functions defined by Eq. A15
k_ω = thermal conductivity of ω phase
K = ratio of heat capacities of solid and fluid phases, Eq. 4
K_{eff} = effective conductivity of packed bed under no-flow conditions
K^*_{zz}, K^*_{yy} = longitudinal and lateral effective thermal conductivities in packed bed
Nu, Nu_f = Nusselt numbers based on an overall and a film heat transfer coefficient, respectively, Eqs. 6, 9
Pe_p = Peclet number based on the pore hydraulic radius, Eq. 8
$S_{\beta\beta}$, $S_{\beta\sigma}$ = terms contributing to the pulse separation between phases, Eq. 5
t = Time
t_ω = mean residence time for the breakthrough curve for phase ω at a given axial location
T = temperature
$\langle T_\omega\rangle^\omega$ = intrinsic phase-averaged temperature for ω phase
u_ω = pulse velocity of ω phase
$\langle v_\beta\rangle^\beta$ = interstitial fluid velocity in bed
y = position perpendicular to bed axis
Y = dimensionless position perpendicular to bed axis
z = position along bed axis

Greek Letters

α_ω = thermal diffusivity of ω phase
(α^*_{zz}), (α^*_{yy}) = longitudinal and lateral thermal dispersivity of packed bed
$(\alpha^*_{zz})_\omega$ = longitudinal thermal dispersivity measured from ω phase temperature response
Δ = separation between fluid and solid temperature resonses, Eq. 28
ϵ_ω = volume fraction of ω phase in packed bed
κ = ratio of thermal conductivities of solid and fluid, Eq. 10

λ,ξ = dummy variables, Eqs. A8, A12
η = dimensionless radial position, Eq. A6
ρ_ω = density of ω phase
$\langle\rho\rangle$ = average bed density $\epsilon_\beta\rho_\beta + \epsilon_\sigma\rho_\sigma$
τ = dimensionless time, Eq. A5
θ = dimensionless temperature in solid particle, Eq. A7

Subscripts

ω = refers to fluid phase (β) and solid phase (σ)
n = index referring to nth term in series, Eq. A8
s = surface of particle
c = center of particle
o = low temperature or initial bed temperature
1 = high temperature or final bed temperature

LITERATURE CITED

Dixon, A. G., and D. L. Cresswell, "Theoretical Prediction of Effective Heat Transfer Parameters in Packed Beds," *AIChE J.*, **25**, 663 (1979).

Eidsath, A., et al., "Dispersion in Pulsed Systems. III: Comparison between Theory and Experiment for Packed Beds," *Chem. Eng. Sci.*, **38**, 1803 (1983).

Gunn, D. H., and J. F. C. De Souza, "Heat Transfer and Axial Dispersion in Packed Beds," *Chem. Eng. Sci.*, **29**, 1,363 (1974).

Gunn, D. J., and M. Khalid, "Thermal Dispersion and Wall Heat Transfer in Packed Beds," *Chem. Eng. Sci.*, **30**, 261 (1975).

Han, N., J. Bhakta, and R. G. Carbonell, "Longitudinal and Lateral Dispersion in Packed Beds: Effect of Column Length and Particle Size Distribution," *AIChE J.* (Feb., 1985).

Kunii, D., and N. Ono, "Heat Transfer from Wall Surface to Packed Beds at High Reynolds Number," *J. Chem. Eng.*, (Japan) **1**, 21 (1968).

Levec, J. and R. G. Carbonell, "Longitudinal and Lateral Thermal Dispersion in Packed Beds. I: Theory," *AIChE J.*, **31**(4), 543 (Apr., 1985).

Nozad, I., "Effect Thermal Conductivities for Two- and Three-Phase Systems: A Theoretical and Experimental Study," Ph.D. Thesis, Dept. Chem. Eng., Univ. California, Davis (1983).

Ryan, D., R. G. Carbonell, and S. Whitaker, "A Theory of Diffusion and Reaction in Porous Media," *AIChE Symp. Ser.* No. 202, 77, 46 (1981).

Sáez, A. E., and B. J. McCoy, "Dynamic Response of a Packed Bed Thermal Storage System—A Model for Solar Air Heating," Solar Energy **29**, 201 (1982).

Schlünder, E. V., "Transport Phenomena in Packed Bed Reactors," *Chemical Reaction Engineering Reviews*, D. L. Houston and V. W. Weekman, Jr., Eds., ACS Symp. Ser. No. 72, Am. Chem. Soc., Washington, DC (1978).

Vortmeyer, D. and R. Beninger, "Comments on the Paper: Theoretical Prediction of Effective Heat Transfer Parameters in Packed Beds by Anthony Dixon and D. L. Cresswell [*AIChE J.*, **25**, 663 (1979)]" *AIChE J.*, **28**, 508 (1982).

Wakao, N., S. Kaguei, and T. Funazkri, "Effect of Fluid Dispersion Coefficients on Particle-to-Fluid Heat Transfer Coefficients in Packed Beds," *Chem. Eng. Sci.*, **34**, 325 (1979).

Whitaker, S., "Forced Convection Heat Transfer Correlations for Flow in Pipes, Past Flat Plates, Single Cylinders, Single Spheres, and for Flow in Packed Beds and Tube Bundles," *AIChE J.*, **18**, 361 (1972).

Yagi, S., D. Kunii, and N. Wakao, "Studies on Axial Effective Thermal Conductivities in Packed Beds," *AIChE J.*, **6**, 543 (1960).

Zanotti, F., and R. G. Carbonell, "Development of Transport Equations for Multiphase Systems. III: Application to Heat Transfer in Packed Beds," *Chem. Eng. Sci.* **39**, 299 (1984).

Manuscript received Apr. 11, 1983, and accepted Mar. 1, 1984.